Molecular Therapy
Nucleic Acids
Original Article

Chimeric RNA-binding protein-based killing switch targeting hepatocellular carcinoma cells

Jiong Yang[1,2] and Shigang Ding[1,2]

[1]Department of Gastroenterology, Peking University Third Hospital, Beijing 100191, China; [2]Beijing Key Laboratory for Helicobacter Pylori Infection and Upper Gastrointestinal Diseases, Beijing 100191, China

Cancer cell-specific killing switches are synthetic circuits developed as an intelligent weapon to specifically eliminate malignant cells. RNA-delivered synthetic circuits provide safer means to control oncolytic functions, in which proteolysis-responding capsid-cNOT7 is developed to enable logic computation and modular design. Unfortunately, although circuits containing these capsid-cNOT7s exhibited good performance when introduced as replicons, in modified mRNA (modRNA) delivery, the performance was not quite as good. To improve this situation, alternative modules suitable for modRNA delivery need to be developed. An attractive option is RNA-binding protein (RBP)/riboswitches. In this study, RBPs were engineered by fusing with degron and cleavage sites. The compatibility of these chimeric RBPs with proteolysis-based sensing units were tested. Eight two-input logic gates and four three-input logic gates were implemented. After building this chimeric RBP-based system, we constructed a hepatocellular carcinoma (HCC) cell-specific killing circuit using two proteolysis-based sensing units, a two-input logic OR gate, and a leak-proof apoptosis-inducing actuator, which distinguished HCC cells and induced apoptosis in a mixed IMR90-PLC/PRF/5 population.

INTRODUCTION

Cancer cell-specific killing switches are synthetic circuits developed to specifically eliminate malignant cells while sparing healthy cells through cell classifiers, which can perform logic computation based on multiple cancer signatures and activate therapeutic actuators.[1] Combined with small molecules or optogenetic sensing units, precise control of therapeutic outputs can be achieved, making it a promising anticancer approach.[2,3]

Compared with synthetic DNA, synthetic messenger RNA (mRNA) provides safer means to control programmed functions without causing random genomic integration.[4–6] Replicon and modified mRNA (modRNA) platforms are commonly used in RNA-delivered synthetic circuits.[7] Derived from the genome of RNA viruses, the replicon is a self-amplifying mRNA. For circuits that require prolonged protein expression, the replicon is a good option. However, for applications benefitting from transient protein expression, such as killing switches, the long-lasting protein expression driven by the replicon becomes a burden, which puts transfected cells at potential risk. In this situation, short-lived modRNAs that can be naturally degraded are more appropriate. The long RNA length (about a 7,500-nt nonstructural protein [nsP] coding sequence apart from the variable region of interest) of the replicon may make it more challenging to produce high-quality RNAs compared with modRNAs, because for *in vitro* transcription, large synthesizing transcripts require extra GTP to avoid low yield or premature termination of transcription, which affects the fraction of transcripts capped, leading to rapid degradation.[8] Compared with modRNAs, a virus-derived replicon might cause elevated inflammation. Additionally, the interaction between nonstructural proteins and host factors still remains to be addressed.[9]

Many synthetic circuits have been designed for RNA-only delivery, among which chimeric proteins called capsid-cNOT7s are frequently used.[10–12] Capsids such as MS2 bacteriophage coat protein (MS2CP) and PP7 bacteriophage coat protein (PP7CP) are RNA-binding proteins (RBPs) that recognize corresponding aptamers in the 3′ UTR of target mRNAs. cNOT7 is a deadenylase that can inhibit the translation and promote the degradation of target mRNAs.[13] Capsid-CS-cNOT7 is constructed by inserting protease cut sites (CSs) at the hinge area of capsid-cNOT7. With the presence of corresponding proteolytic activity, the CS is cleaved, causing the release of cNOT7 and relieving target mRNAs from repression. Degron plays an important role in regulating protein degradation. When connected with capsid-cNOT7 via a CS, the degron can increase the degradation of capsid-cNOT7. Once the CS is cleaved by protease, the degron will be removed, leaving stable capsid-cNOT7.[11] The capsid-cNOT7-based system has three advantages: (1) coupled with respective aptamers in the 3′ UTR of target mRNAs, the output controlled by capsid-cNOT7 is very flexible, such as secreting protein, membrane protein, and plasma protein; (2) with a series of capsids possessing good orthogonality, capsid-cNOT7 can control different outputs to form various circuit topologies; and (3) after engineered by adding a

Received 6 December 2020; accepted 13 August 2021;
https://doi.org/10.1016/j.omtn.2021.08.012.

Correspondence: Jiong Yang, Department of Gastroenterology, Peking University Third Hospital, Beijing 100191, China.
E-mail: yangjiong@bjmu.edu.cn
Correspondence: Shigang Ding, Department of Gastroenterology, Peking University Third Hospital, Beijing 100191, China.
E-mail: dingshigang222@163.com

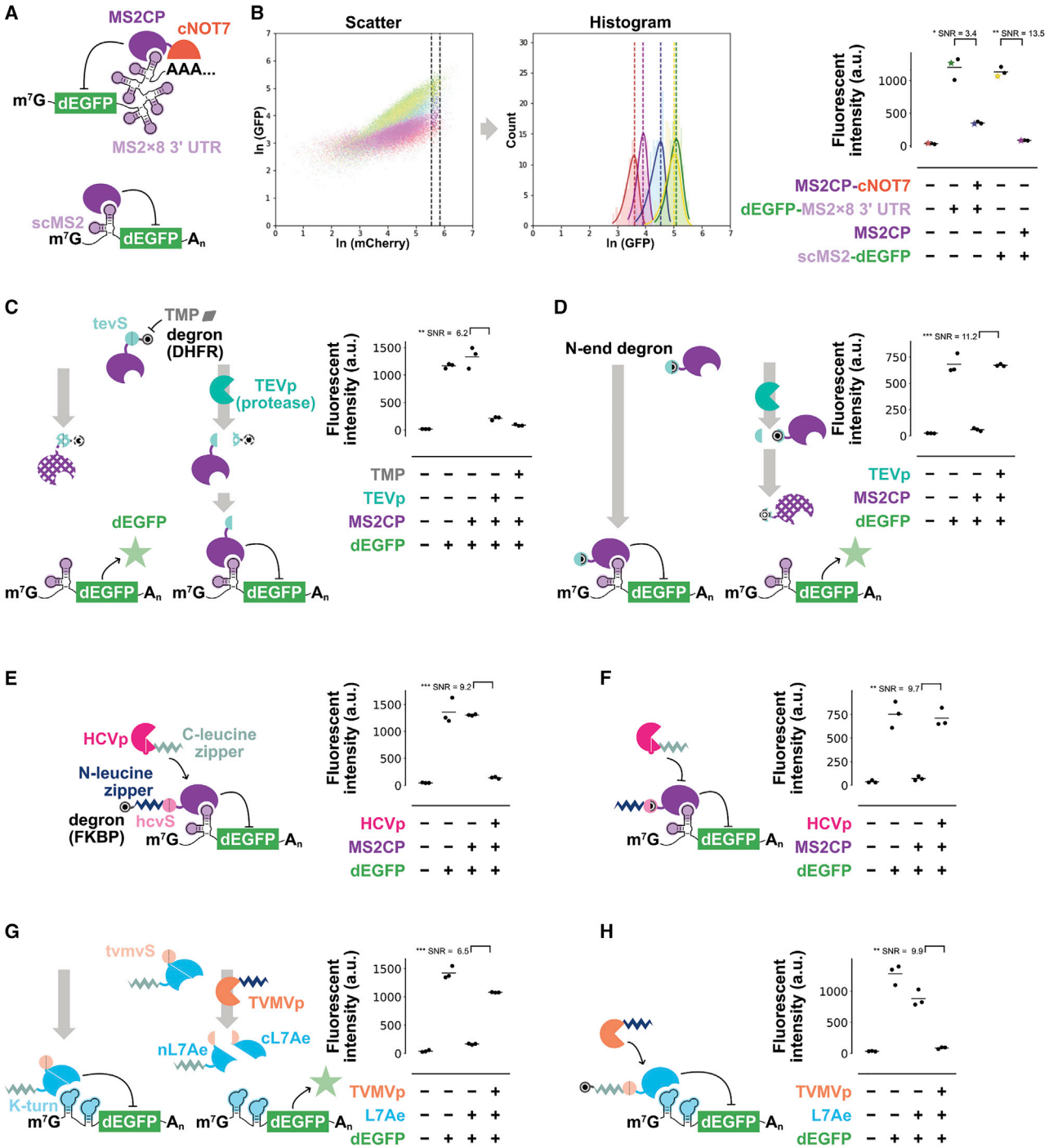

Figure 1. Engineering proteolysis/drug-responsive MS2CP and proteolysis-responsive L7Ae

(A) Schematic representation of two NOT gates. The upper gate was constructed with MS2CP-cNOT7 while the lower gate was constructed with the MS2CP-scMS2 pair. (B) Five groups of synthetic circuits were transferred into 293T cells as modRNAs. Cells were analyzed by flow cytometry. dEGFP was used for signal fluorescence while mCherry was used as a co-transfection marker. The results of five log-log flow cytometry representative scatterplots were merged in the left graph: red scatterplots represent the negative control; green scatterplots represent the result with dEGFP-MS2×8 3′ UTR but without MS2CP-cNOT7; blue scatterplots represent the result with dEGFP-MS2×8 3′ UTR and MS2CP-cNOT7; gold scatterplots represent the result with scMS2-dEGFP but without MS2CP; purple scatterplots represent the result with scMS2-dEGFP and MS2CP. The mCherry expression gate of 98 and 99.5 percentiles are shown between dashed lines. Data acquired between the dash lines are shown in the histogram and fitted with skewed Gaussian distribution. The fluorescence intensity of each group is presented in the right graph. The short horizontal line indicates data from the panel. a.u.,

(legend continued on next page)

CS and degrons, capsid-cNOT7 can integrate signals from different formerly established proteolysis-based sensing units and carry out logic computation. These proteolysis-based sensing units are essential in transducing various signals into the synthetic circuit through proteolytic activities, enabling modular design. Unfortunately, although circuits containing capsid-cNOT7 exhibited good performance when introduced as replicons, when introduced as modRNAs, the performance was not quite as good.[11,12] To improve this situation, alternative modules suitable for modRNA delivery need to be developed.

A particularly attractive option is RBPs/riboswitches, which can achieve flexible output control and various circuit topologies.[14] However, currently reported RBPs lack the versatile ability to integrate multiple protease cleavage activities such as capsid-cNOT7. In this study, we engineered a series of chimeric RBPs, which, along with responsive riboswitches, can integrate cleavage signals and implement logic gates. We also tested the compatibility of these chimeric RBPs with proteolysis-based sensing units constructed in our previous study, such as drug sensing (abscisic acid [ABA] and rapamycin [Rapa]), blue light sensing, Hippo sensing, and alpha-fetoprotein (AFP) sensing. Eight two-input logic gates (AND, OR, NAND, NOR, XOR, XNOR, IMPLY, and NIMPLY) were implemented using the chimeric RBPs in mammalian cells. Additionally, four three-input logic gates (AND, OR, NAND, and NOR) were implemented to verify the scalability of the system. Finally, a hepatocellular carcinoma (HCC) cell-specific killing circuit was constructed by combining two proteolysis-based sensing units, a two-input logic OR gate and an apoptosis-inducing actuator. Our newly engineered devices expanded the foundational toolset for designing synthetic circuits in modRNA delivery. Additionally, the engineering of MS2CP is realized through directly adding a CS and degrons in the N-end and C-end of this protein without relying on the protein analysis work to confirm the location of innate CSs. This design concept expands the candidate protein pool for logic computation. This chimeric RBP-based system is compatible and scalable, indicating versatile applicable potential in oncolytic therapy.

RESULTS

Engineering proteolysis-responsive chimeric RBPs

MS2CP-cNOT7 could repress target mRNAs containing MS2 aptamers in the 3′ UTR. After binding scaffold MS2 riboswitch (scMS2) in the 5′ UTR of target mRNAs, MS2CP could repress the translation of downstream genes.[15–17] The performance of NOT gates constructed with the MS2CP-cNOT7 or MS2CP-scMS2 pair (Figure 1A) in modRNA delivery was compared (Figure 1B). The repression efficiency of the MS2CP-scMS2 pair-based circuit was much better than that of the MS2CP-cNOT7-based circuit, which encouraged us to develop circuits with RBP/riboswitch pairs. We then started to engineer proteolysis-responsive chimeric RBPs. Tobacco etch virus protease (TEVp) is a highly sequence-specific cysteine protease, the activity of which can be controlled by small molecules or blue-light pulses after a split design.[18–20] To specifically link TEVp activity to MS2CP, we engineered a chimeric RBP in which a TEVp cleavage site (tevS) was inserted between MS2CP and a dihydrofolate reductase (DHFR),[21] the degradation of which could be inhibited by trimethoprim (TMP) and serve as a positive control. The chimeric protein MS2CP-tevS-degron was tested in 293T cells on dEGFP reporters with scMS2 (Figure 1C). Another chimeric MS2CP was also engineered by fusing MS2CP with an N-end degron possessing a tevS (tevD), the destabilizing N-terminal residue of which can only be exposed after TEVp cleavage.[22,23] This tevD-MS2CP, together with TEVp and reporters, formed another synthetic circuit responding to TEVp cleavage (Figure 1D).

To enable the design of multi-input processing circuits, chimeric MS2CP responding with another viral protease possessing good orthogonality was needed. For this purpose, we engineered MS2CP to respond with the cleavage of hepatitis C virus protease (HCVp).[24,25] An antiparallel heterodimerizing N-leucine zipper (NZ) followed with a HCVp cleavage site (hcvS) was inserted between the FKBP degron and MS2CP to generate a chimeric MS2CP (degron-NZ-hcvS-MS2CP),[26] while its complementary C-leucine zipper (CZ) was incorporated to the N-end of HCVp, thus enhancing the protease ability to dock with and cleave its MS2CP target.[27] Results showed that cells transfected with HCVp successfully decreased dEGFP abundance, indicating that the circuit responded well to HCVp (Figure 1E). Another HCVp-responding MS2CP was engineered by fusing MS2CP with an NZ and an N-end degron possessing a hcvS (hcvD), the destabilizing N-terminal residue of which could only be exposed after HCVp cleavage. Results showed that this NZ-hcvD-MS2CP responded well to HCVp cleavage (Figure 1F).

The design of complex synthetic circuits required more RBPs to control different outputs, so we next focused on L7Ae, an RBP that binds

arbitrary units (n = 3). Stars represent the dEGFP fluorescence intensity of each group in the first test, as the vertical dashed line in the middle graph is shown with the same color. The signal-to-noise ratio (SNR) is shown here and in the following figures. (C) Schematic representation of synthetic circuits with engineered TEVp/TMP-responsive MS2CP and the fluorescence intensity of each group. The MS2CP was engineered by adding tevS, which could be cleaved by TEVp, and degron, which could be inhibited by TMP to the C-end of the protein. (D) Schematic representation of MS2CP engineered with the N-end degron and the fluorescence intensity of each group. The degron could be exposed after the cleavage of TEVp, which causes the subsequent degradation of MS2CP. (E) Schematic representation of engineered HCVp-responsive MS2CP and the fluorescence intensity of each group. The MS2CP can only be stable to suppress the translation of dEGFP after the cleavage of hcvS. (F) Schematic representation of another engineered HCVp-responsive MS2CP and the fluorescence intensity of each group. After the cleavage of hcvS, the degron is exposed, MS2CP is degraded, and the translation suppression of dEGFP is alleviated. (G) Schematic representation of engineered TVMVp-responding L7Ae and the fluorescence intensity of each group. After the cleavage of tvmvS, L7Ae is split into nL7Ae and cL7Ae, either of which lost the suppression character, so the dEGFP intensity is rescued with the presence of TVMVp. (H) Schematic representation of another engineered TVMVp-responding L7Ae and the fluorescence intensity of each group. Without the cleavage of TVMVp, L7Ae is degraded and alleviates the suppression of dEGFP translation. Welch's t test was used to evaluate significant differences: *$p < 0.05$, **$p < 0.01$, ***$p < 0.001$; ns, not significant.

the classical kink-turn (Kt) riboswitch.[28] Based on analyzing the crystal structure of L7Ae, Cella et al.[10] identified insertion points to harbor a tevS without affecting the behavior of L7Ae. On this basis, we designed a chimeric L7Ae responding to tobacco vein mottling virus protease (TVMVp) by inserting a TVMVp cleavage site (tvmvS).[29] A CZ was fused at the N-end of L7Ae (CZ-nL7Ae-tvmvS-cL7Ae) while the complementary NZ was fused at the C-end of TVMVp to enhance the proteolytic activity. Results showed that TVMVp effectively increased the reporter intensity (Figure 1G). We also fused a degron following a CZ and a tvmvS to L7Ae, constructing another chimeric L7Ae (degron-CZ-tvmvS-L7Ae) (Figure 1H).[26]

Synthetic circuits constructed in this study were introduced into cells as modRNAs. The amounts of transfected modRNAs were optimized through testing and analyzing the reporter fluorescent intensity across 24 groups of concentration combinations of RBP and corresponding proteases (Figure S1). The robustness of the system is demonstrated in Figures S2A–S2F. Because TMP is toxic to mammalian cells, which might influence fluorescence intensity, further experiments were conducted. Although TMP slightly decreased the fluorescence intensity and cell viability, there was no statistical significance (Figures S2G and S2H).

Testing the compatibility of chimeric RBPs with proteolysis-based sensing units

Composability has been considered as a key challenge in developing larger systems to achieve predictable behavior, the premise of which depends on the compatibility of the biological parts.[30] Hence, in the next study, we tested the compatibility of our newly engineered chimeric RBPs with proteolysis-based sensing units constructed with split-designed proteases and riboswitches, which could transduce protein-protein interactions (PPIs) or the abundance of certain proteins into proteolytic activities.[20,31] For killing switches, this sensing ability is crucial in detecting tumor biomarkers or introducing exogenous control. The chimeric tevD-MS2CP successfully connected with our previously reported ABA sensing nTEVp-PLY-T2A-ABI-cTEVp module and optogenetic nTEVp-CIBN-T2A-CRY2-cTEVp module (Figures 2A and 2B). The heterodimerization of ABI and PLY is inducible with ABA. In the nTEVp-PLY-T2A-ABI-cTEVp module, the N-terminal part of TEVp (nTEVp) was fused with PLY, while the C-terminal part of TEVp (cTEVp) was fused with ABI. With the existence of ABA, PLY interacted with ABI, which made nTEVp and cTEVp spatially close enough to resume the proteolytic activity to cleave tevS. CIBN is the N-terminal fragment (residue 1–170) of CIB1, which is commonly used to promote the light-dependent interaction with CRY2. In the nTEVp-CIBN-T2A-CRY2-cTEVp module, nTEVp was fused with CIBN, which could interact with CRY2 under the stimulation of blue light, while cTEVp was fused with CRY2. When stimulated with blue light, CIBN interacted with CRY2, which resumed the proteolytic activity of TEVp. Similarly, CZ-nL7Ae-tvmvS-cL7Ae, together with the Rapa-sensing nTVMVp-FRB-T2A-FKBP-cTVMVp-NZ module and reporters, formed Rapa-sensing synthetic circuits (Figure 2C). The heterodimerization of FKBP and FRB is inducible with Rapa. In the nTVMVp-FRB-T2A-FKBP-cTVMVp-NZ module, the N-terminal part of TVMVp (nTVMVp) was fused with FRB while the C-terminal part of TVMVp (cTVMVp) was fused with FKBP. With the presence of Rapa, FRB interacted with FKBP, which made nTVMVp and cTVMVp spatially close enough to resume its proteolytic activity. Then, we tested the compatibility of MS2CP-tevS-degron with the Hippo-sensing module nTEVp-YAP-T2A-14-3-3-cTEVp. The negative regulator of YAP1 plays a pivotal role in the Hippo signaling pathway. In the core cascade of this pathway, STK3 phosphorylates and activates LATS1, which, in complex with MOB1, phosphorylates and inactivates YAP1 oncoprotein. The phosphorylation of YAP1 mediated by LATS1 results in its association with 14-3-3 and inhibits its translocation into the nucleus to regulate genes important for cell death, cell proliferation, and cell migration.[32] In the nTEVp-YAP-T2A-14-3-3-cTEVp module, nTEVp was fused with YAP while cTEVp was fused with 14-3-3. At the Hippo ON state, YAP1 was phosphorylated and interacted with 14-3-3, which resumed TEVp activity, while at the Hippo OFF state, the phosphorylation of YAP1 was inhibited, and so was the interaction between YAP1 and 14-3-3. Results showed that the depletion of LATS1 or MOB1B successfully increased the reporter signal, and the depletion of YAP1 served as a positive control. Conversely, overexpressing STK3 and LATS1, either in combination or alone, decreased the reporter intensity (Figure 2D; Figures S8A–S8E). Another synthetic circuit was established with AFP-riboswitch-CZ-HCVp, degron-NZ-hcvS-MS2CP, and reporters. In the AFP-riboswitch-CZ-HCVp module, riboswitches containing AFP aptamers were used to control the expression of CZ-HCVp, which could cleave hcvS. When AFP bound with AFP aptamer, the expression of CZ-HCVp was inhibited. In 293T cells, overexpressing AFP strongly increased the reporter intensity while in PLC/PRF/5 cells where AFP was highly expressed, AFP RNAi decreased the reporter intensity (Figure 2E; Figure S8F). These results demonstrated good compatibility of chimeric RBPs with proteolysis-based sensing units, which enabled the synthetic circuits with versatile functions.

Construction of logic gates composed of the chimeric RBPs

We then designed core circuit functions for cell classifiers to integrate signals, starting with two-input logic gates. The Boolean logic implemented by chimeric RBPs responded to the cleavage of proteases and mRNAs with corresponding riboswitches in the 5′ UTR (Figure 3A). Asunaprevir (ASV) is an inhibitor of HCVp.[33] The activities of TEVp were controlled by ABA. First, the combination of formerly engineered MS2CPs was able to implement four two-input logic gates: (1) tevD-MS2CP and NZ-hcvD-MS2CP can implement the AND logic gate (Figure 3B; Figure S3A); (2) degron-NZ-hcvS-MS2CP and MS2CP-tevS-degron can implement the NOR logic gate (Figure 3E; Figure S3D); (3) NZ-hcvD-MS2CP and MS2CP-tevS-degron can implement the HCVp NIMPLY TEVp logic gate (Figure 3I; Figure S4D); and (4) tevD-MS2CP and degron-NZ-hcvS-MS2CP can implement the TEVp NIMPLY HCVp logic gate (Figure 3K; Figure S5B). Second, to implement more logic gates, MS2CP was further engineered to harbor two cleavage sites and the corresponding degrons: (1) tevD-NZ-hcvD-MS2CP was constructed to implement the OR logic gate, because the cleavage of either site was sufficient

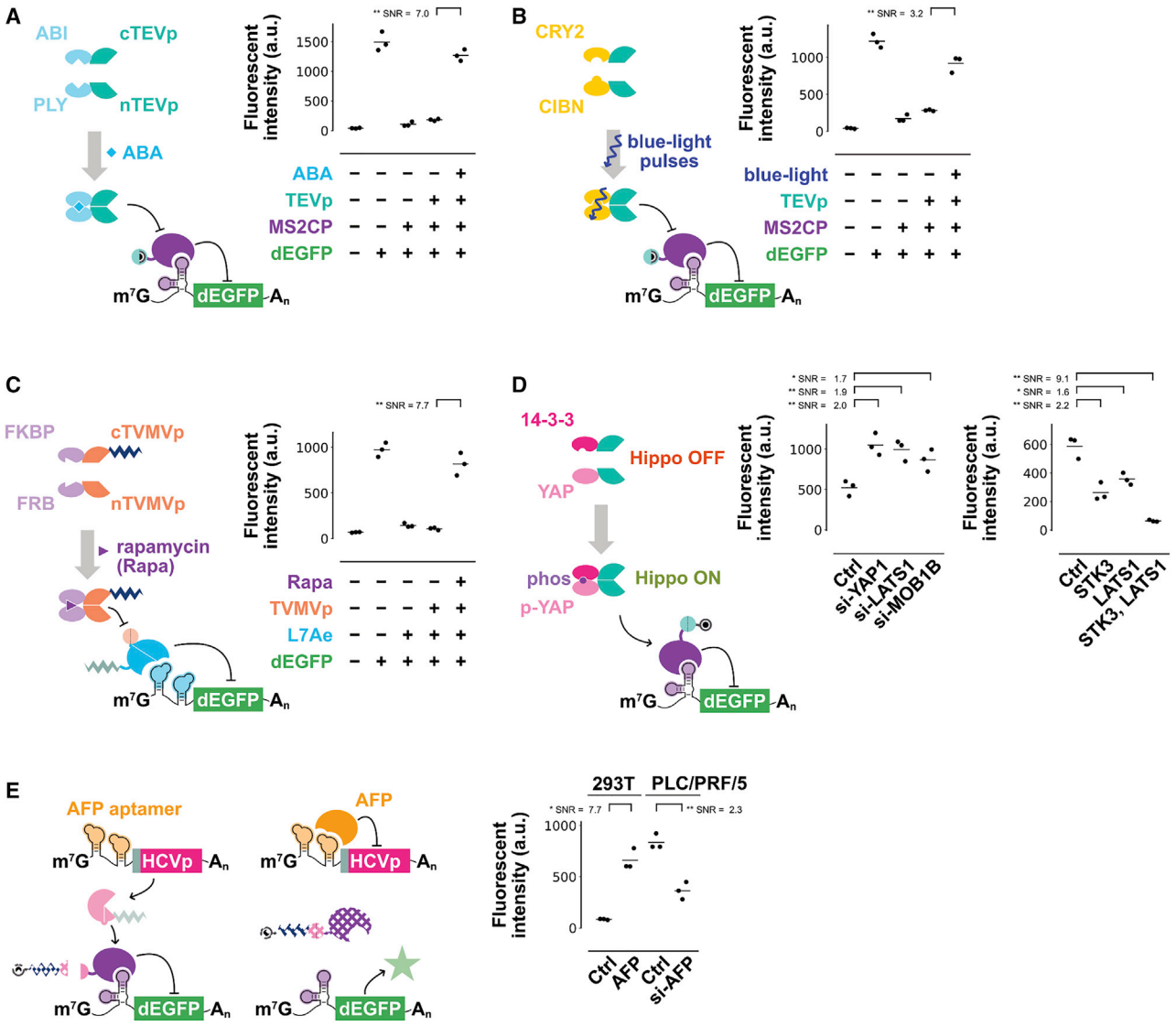

Figure 2. Synthetic circuits composed of engineered chimeric RBPs and proteolysis-based sensing units

(A) Schematic representation of synthetic circuit composed of ABA-responsive TEVp, tevD-MS2CP, and scMS2-dEGFP reporter. Results show high fluorescence intensity with the presence of both ABA and ABA-responsive TEVp, similar to the dEGFP positive control. (B) Schematic representation of synthetic circuit composed of nTEVp-CIBN-2A-CRY2-cTEVp, tevD-MS2CP, and scMS2-dEGFP reporter. Result shows high fluorescence intensity with the presence of both nTEVp-CIBN-2A-CRY2-cTEVp and blue-light pulses. (C) Schematic representation of synthetic circuit composed of Rapa-responsive TVMVp, CZ-nL7Ae-tvmvS-cL7Ae, and Kt-dEGFP reporter. Result shows high fluorescence intensity with the presence of both Rapa and Rapa-responsive TVMVp. (D) Schematic representation of synthetic circuit composed of nTEVp-YAP, 14-3-3-cTEVp, MS2CP-tevS-degron, and scMS2-dEGFP reporter. The depletion of YAP1, LATS1, or MOB1B by RNA interference (RNAi) successfully increased the dEGFP signal. The dEGFP intensity was decreased in the STK3 and LATS1 overexpression group, either in combination or alone. (E) Schematic representation of synthetic circuit composed of AFP-riboswitch-CZ-HCVp, degron-NZ-hcvS-MS2CP, and scMS2-dEGFP reporter. Results show that overexpressing AFP significantly increased dEGFP intensity in 293T cells loaded with the circuit, while in PLC/PRF/5 cells, AFP RNAi decreased dEGFP intensity. Welch's t test was used to evaluate significant differences: *$p < 0.05$, **$p < 0.01$, ***$p < 0.001$; ns, not significant.

to destabilize MS2CP (Figure 3C; Figure S3B); (2) degron-NZ-hcvS-MS2CP-tevS-degron was constructed to implement the NAND logic gate, in which MS2CP could only be stabilized with the existence of both HCVp and TEVp (Figure 3D; Figure S3C); (3) tevD-MS2CP-NZ-hcvS-degron was constructed to implement the HCVp IMPLY TEVp logic gate, in which MS2CP was stabilized with the existence of HCVp but without TEVp (Figure 3H; Figure S4C); and (4) NZ-hcvD-MS2CP-tevS-degron was constructed to implement the TEVp IMPLY HCVp logic gate, in which MS2CP was stabilized with the existence of TEVp but without HCVp (Figure 3J; Figure S5A). Third, to provide the full set of two-input Boolean logic, the four engineered MS2CPs were utilized in combination: (1) tevD-NZ-hcvD-MS2CP

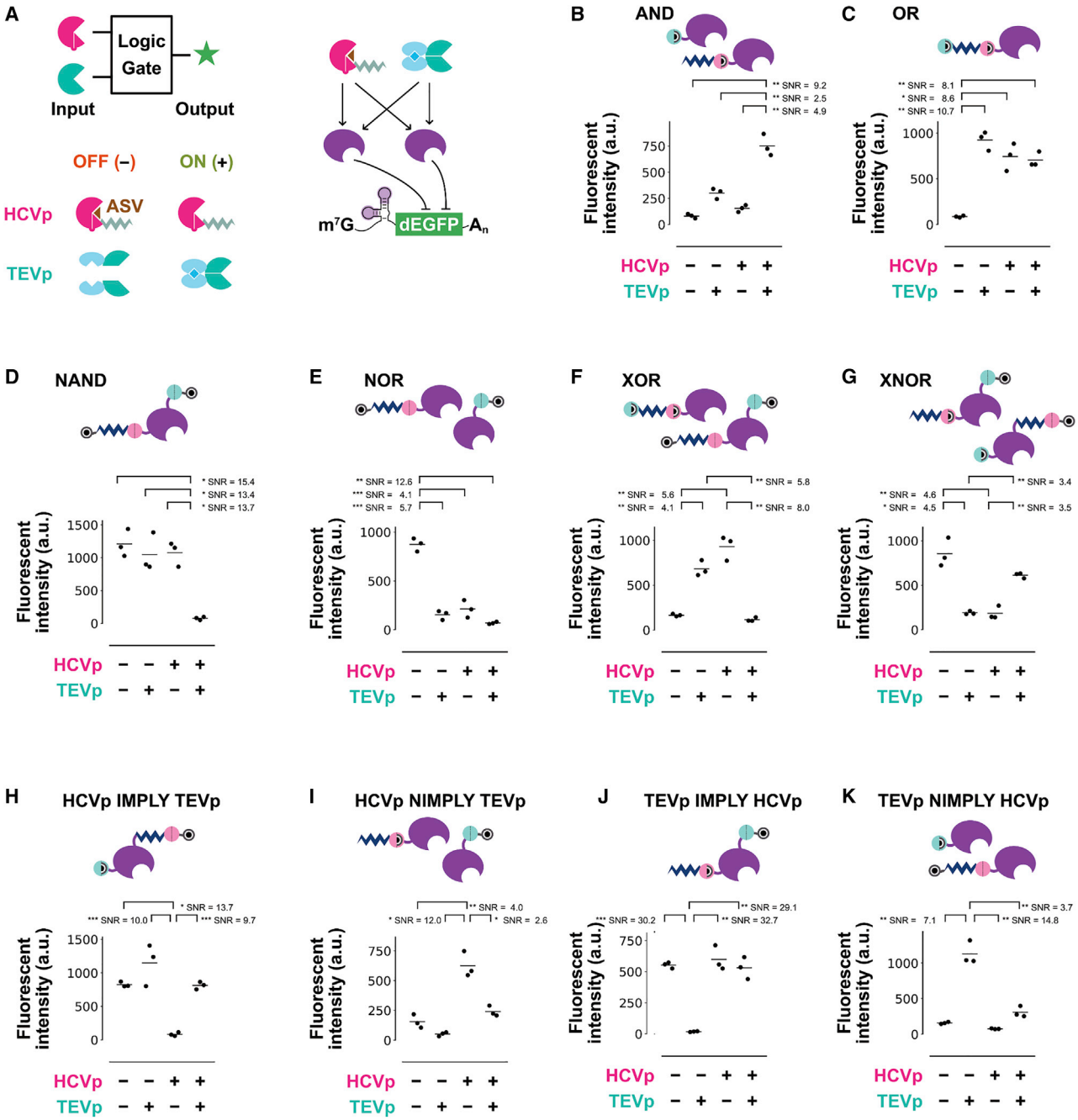

Figure 3. Eight different two-input logic circuits constructed with the engineered MS2CP

(A) Schematic representation of two-input logic circuits sensing HCVp and TEVp. The activities of HCVp and TEVp are controlled by small molecules. In the presence of ASV, the state of HCVp is OFF (–), while without ASV, the state of HCVp is ON (+). In the presence of ABA, the state of TEVp is ON (+), while without ABA, the state of TEVp is OFF (–). (B–K) Components of AND, OR, NAND, NOR, XOR, XNOR, HCVp IMPLY TEVp, HCVp NIMPLY TEVp, TEVp INMPY HCVp, and TEVp NIMPLY HCVp logic gates and the fluorescence intensity of each group. Welch's t test was used to evaluate significant differences: *p < 0.05, **p < 0.01, ***p < 0.001; ns, not significant.

and degron-NZ-hcvS-MS2CP-tevS-degron can implement the XOR logic gate (Figure 3F; Figure S4A); and (2) NZ-hcvD-MS2CP-tevS-degron and tevD-MS2CP-NZ-hcvS-degron can implement the XNOR logic gate (Figure 3G; Figure S4B).

Furthermore, MS2CP coding mRNAs with Kt in the 5′ UTR was used to combine the previously engineered L7Ae and MS2CP. On the basis of the two-input logic gates described above, we generated more complex circuits that could respond to the proteolysis activities of HCVp,

TEVp, and TVMVp, implementing three-input logic gates (Figure 4A): (1) tevD-MS2CP, NZ-hcvD-MS2CP, degron-CZ-tvmvS-L7Ae, and Kt-MS2CP were combined to implement the three-input AND logic gate that output a positive dEGFP signal only when all three proteases were active (Figure 4B; Figure S6A); (2) degron-CZ-tvmvS-L7Ae and Kt-tevD-NZ-hcvD-MS2CP were combined to implement the three-input OR logic gate that output a negative dEGFP signal only when all three proteases were inactive (Figure 4C; Figure S6B); (3) CZ-nL7Ae-tvmvS-cL7Ae and Kt-degron-NZ-hcvS-MS2CP-tevS-degron were combined to implement the three-input NAND logic gate that output a negative dEGFP signal only when all three proteases were active (Figure 4D; Figure S7A); and (4) degron-NZ-hcvS-MS2CP, MS2CP-tevS-degron, CZ-nL7Ae-tvmvS-cL7Ae, and Kt-MS2CP were combined to implement the three-input NOR logic gate that output a positive dEGFP signal only when all three proteases were inactive (Figure 4E; Figure S7B).

Building an HCC cell-specific killing switch using the constructed two-input logic gates

Although the newly designed module exhibited good performance in modRNA delivery, fluorescent signals were still detected at OFF states, indicating the existence of output leakage. For killing switches, this leakage will cause unwanted death. It is necessary to introduce an inhibitory mechanism into the system to alleviate the leaking toxicity to these untargeted cells. Thus, we constructed a leakproof apoptosis-inducing actuator responding to MS2CP, which was composed of two engineered mRNAs: (1) an scMS2-PP7CP-T2A-Bcl-2 mRNA was engineered by fusing PP7CP with Bcl-2 through T2A peptides and adding scMS2 in the 5′ UTR; and (2) the corresponding scPP7-hBax mRNA was engineered by adding scPP7 in the 5′ UTR. Human Bax (hBax) was set as the endpoint output while Bcl-2 behaved as a buffer to repress the apoptosis caused by leaky hBax in OFF states.[14,15,34] To verify the composability between the engineered chimeric RBPs and the actuator, they were combined with the two-input logic OR gate (Figure 3C) to generate an apoptosis-regulatory synthetic circuit (Figure 5A). The circuit was transfected into 293T cells to test the response of proteases. 24 h after the transfection, cells were stained with SYTOX red for dead cells while annexin V was used for apoptotic cells to assess apoptosis level. Results showed that the circuit only induced apoptosis at the absence of both HCVp and TEVp activities, the apoptosis level of which was comparable to the hBax only group (Figures 5B and 5D). The reduction index was calculated to quantify the effect of proteolytic activities on cell numbers (Figure 5E).[35] Compared with the control condition, the relative reduction in cell numbers sharply increased under the absence of both proteolytic activities (Figure 5F), indicating that the apoptosis-inducing actuator could selectively regulate cell death by sensing the activity of two proteases.

Finally, we rationally designed an HCC cell-specific killing switch by combining two proteolysis-based sensing units, the two-input logic OR gate (Figure 3C) and the leakproof apoptosis-inducing actuator. Two sensing units constructed as shown in Figures 2D and 2E were utilized to sense the state of Hippo pathway and the existence of AFP, two major characters of PLC/PRF/5 cells (Figure 6A).[36,37] Four kinds of PLC/PRF/5 strains established in our previous study were used to verify the function of this synthetic circuit: (1) control strain that was transfected with control vector; (2) AFP knockdown strain; (3) PPP2CA knockdown strain; and (4) AFP and PPP2CA knockdown strain.[31] The circuit specifically induced apoptosis in PLC/PRF/5 control and wild-type groups (Figures 6B and 6C). The reduction index of the control strain and wild-type strain was much higher than that for other groups and IMR90 cells (Figure 6D), indicating that the designed circuit could specifically induce apoptosis in PLC/PRF/5 cells matching the profile of Hippo OFF and AFP expressing. The IMR90 cell line is derived from the lung tissue of a female white fetus (16 weeks old), which has a finite lifespan.[38] Thus, it was chosen as a non-target cell in this research. The expression levels of AFP and PPP2CA are shown in Figure S8G. Furthermore, the circuit specifically killed PLC/PRF/5 cells in a mixed IMR90-PLC/PRF/5 population (Figure 6E). These results demonstrated the utility of our engineered chimeric RBPs in forming programmable therapeutic devices.

DISCUSSION

Most of the synthetic circuits are designed under the principle of the binary system, which means that the output is made to act in only two states, ON and OFF.[39] To maximize the observable range of the reporters, highly transfected cells should be used, which shows the largest separation of basal reporter signal from cellular autofluorescence to reporters.[35] In these highly transfected cells, fluorescent signals can be detected at OFF states, indicating the existence of output leakage. For killing switches, this leakage will cause unwanted death (Figures S9 and S10). It is necessary to introduce a leakproof mechanism into the system to alleviate the leaking toxicity to these untargeted cells. The killing switch reported by Matsuura et al.[15] introduced this mechanism into the circuit, which sensed two microRNAs (miRNAs) and output hBax to selectively eliminate target cells. Our actuator shared a similar structure. For synthetic circuits, upgrading biological parts to improve the functions of formerly constructed frameworks is frequently more beneficial than *de novo* designing a new circuit, because other biological parts have already been developed for the framework to avoid extra labor, and the topology of the circuit can be inherited to simplify the design. Compared with the miRNA-sensing circuit, our killing circuit not only achieved comparable performance, but it also integrated proteolysis-based sensing units that transduced the existence of AFP and the state of the Hippo pathway into the circuit, indicating versatile applicable potential in oncolytic therapy by adapting to different features of tumors.

In our previous study, a capsid-cNOT7-based HCC targeting synthetic circuit was established to distinguish HCC from other cells.[31] This DNA-delivered circuit was stably transfected into cells as plasmids possessing selectable markers. The output of the circuit is anti-VEGF-scFV, which lacks a proper leakproof approach. Although it is a prototype, which confined its application, it developed new modules for sensing the state of the Hippo pathway and the existence

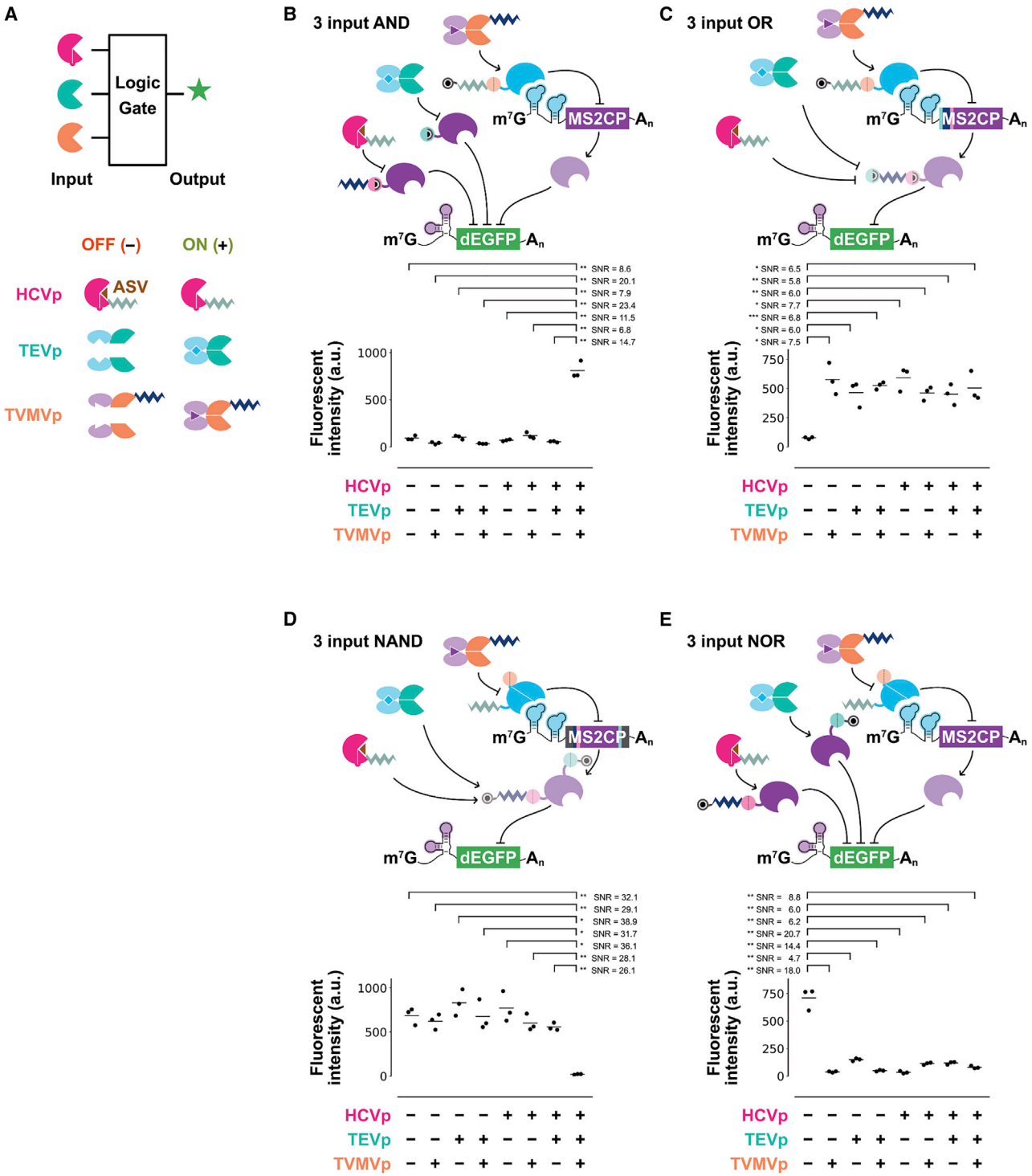

Figure 4. Four different three-input logic circuits constructed with the engineered MS2CP and L7Ae

(A) Schematic representation and explanation of three-input circuits. In the presence of ASV, the state of HCVp is OFF (–), while without ASV, the state of HCVp is ON (+). In the presence of ABA, the state of TEVp is ON (+), while without ABA, the state of TEVp is OFF (–). In the presence of Rapa, the state of TVMVp is ON (+), while without Rapa, the state of TVMVp is OFF (–). (B–E) Schematic representation of synthetic circuits with three-input AND, OR, NAND, and NOR gates and the fluorescence intensity of each group. The activities of proteases are controlled by small molecules. Welch's t test was used to evaluate significant differences: *$p < 0.05$, **$p < 0.01$, ***$p < 0.001$; ns, not significant.

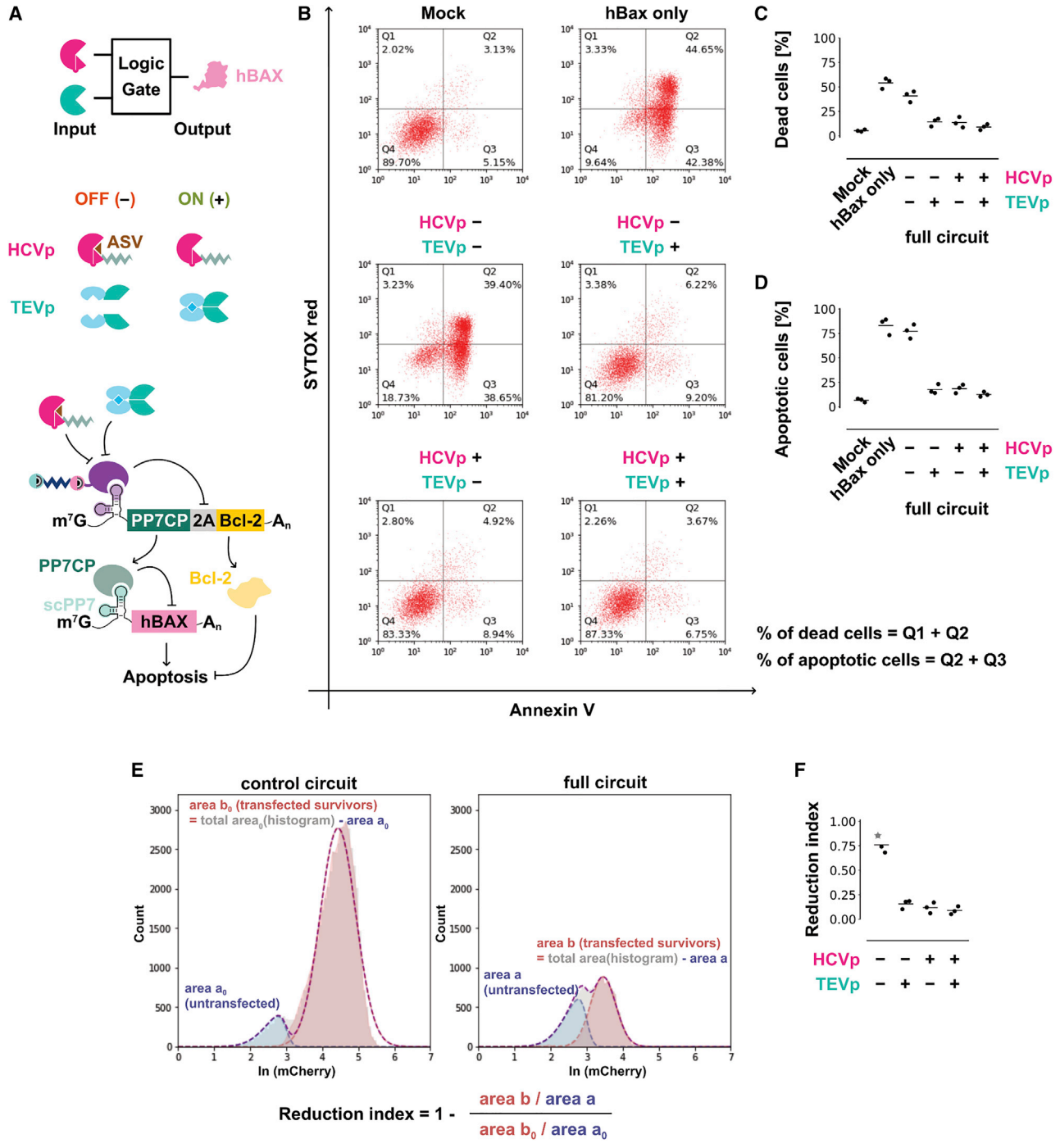

Figure 5. Building the leakproof apoptosis-inducing actuator

(A) Schematic representation of the apoptosis regulatory circuit. The circuit senses HCVp and TEVp as two inputs and has the pro-apoptotic gene *hBax* as the output. PP7CP fused with the anti-apoptotic gene *Bcl-2* through T2A peptides was used to repress apoptosis. (B) Representative two-dimensional flow cytometry data of the apoptosis regulatory circuit. The sum of the Q1 and Q2 fractions, which means SYTOX red positive, represents the percentage of dead cells. The sum of the Q2 and Q3 fractions, which means annexin V positive, represents the percentage of apoptotic cells. (C) Percentage of dead cells of each group. Experiments were repeated three times. (D) Percentage of apoptotic cells of each group. (E) Example of the analysis of the reduction index. As presented in the equation, the reduction index is calculated through comparing the surviving transfected cells numbers in full circuit versus control circuit conditions. The surviving cell number is normalized to the respective untransfected populations. More

(legend continued on next page)

of AFP. These modules were inherited in this study, which proved the compatibility of the newly developed modules. This property is an important virtue because developing a new synthetic module costs considerable resources and time.

In this study, we improved the formerly constructed RNA-delivered synthetic circuit by replacing capsid-cNOT7 with newly engineered chimeric RBPs. The previous design mainly depends on two proteins or domains fusing together as a whole functioning unit to regulate the target mRNA level; for example, capsid takes the binding function while cNOT7 takes the regulatory function. In this situation, the CS can be inserted into the hinge area to proteolytically release the regulatory domain. This design has a limitation that if a protein itself represents a whole function unit, such as MS2CP that emerged in this study, this design strategy is unsuitable to deal with it. One solution is putting the CS into the protein, similar to the design presented in Figure 1G, but this procedure highly relies on the protein analysis work to confirm the location of the innate CS. The design we adopt in this study overcame this limitation by engineering MS2CP through adding the CS and degrons in the N-end and C-end of this protein without changing the innate protein sequence. This design not only extricates logic unit protein from fusion proteins, but it also saved the labor cost in protein analysis and following validation. Using this strategy, suitable proteins can be directly engineered to do logic computation such as MS2CP, expanding the candidate protein pool.

As an important concept of designing synthetic circuits, composability allows predictable interaction of biological parts, which needs to avoid crosstalk.[40–42] There are many proteases with orthogonality similar to TEVp, TVMVp, and HCVp, such as southern bean mosaic virus protease,[43] herpes simplex virus protease,[44] plum pox virus protease,[45] and sunflower mild mosaic virus protease.[46] There are also RBPs similar to MS2CP, L7Ae, and PP7CP, such as LIN28A,[47] U1A-full,[48,49] and phage Com protein.[17] Theoretically, derived synthetic circuits sharing the same orthogonality and topological structures can be constructed using those biological parts. Proteases or RBPs can be expressed by actuator units, which means more complicated synthetic circuits can be constructed through daisy chaining. This composability, along with derived circuits, is the next promising research topic.

MATERIALS AND METHODS

Plasmid construction

Standard procedures were used to generate plasmid constructs. All template plasmids of corresponding modRNAs are included in Table S1. All of the sequences have been uploaded to GenBank.

Cell lines and cell culture

PLC/PRF/5 cells were cultured in 10% fetal bovine serum (FBS)/Eagle's minimum essential medium (EMEM) (Thermo Fisher Scientific, Waltham, MA, USA), with 5% CO_2, at 37°C. 293T and IMR90 cells were cultured in 10% FBS/DMEM (Thermo Fisher Scientific), with 5% CO_2, at 37°C. Five kinds of PLC/PRF/5 strains were established in our previous study:[31] control strain, AFP knockdown strain, PPP2CA knockdown strain, AFP and PPP2CA knockdown strain, and stably EBFP-expressing strain, the culture of which was similar to PLC/PRF/5 cells. The identities of PLC/PRF/5 and 293T cell lines were confirmed by genetic profiling using short tandem repeat (STR) loci and tested for mycoplasma contamination.

Modified RNA preparation and mRNA transfection

The template DNA was generated by PCR for *in vitro* transcription. The T7 promoter was contained in the forward primer while 120-nt-long poly(T) was contained in the reverse primer. PCR products were digested by DpnI restriction enzyme and then purified. A MegaScript T7 kit (Thermo Fisher Scientific) was used to perform *in vitro* transcription under a modified condition, in which GTP was mixed with Anti-Reverse Cap Analog (New England Biolabs, Ipswich, MA, USA) to replace GTP, 5-methylcytosine-triphosphate was used to replace CTP, and pseudouridine triphosphate (TriLink BioTechnologies, San Diego, CA, USA) was used to replace UTP.[12] Transcripts were treated with Turbo DNase (Thermo Fisher Scientific) at 37°C for 30 min and purified with an RNeasy MinElute cleanup kit (QIAGEN, Hilden, Germany). mRNAs were then incubated with Antarctic phosphatase (New England Biolabs) at 37°C for 30 min and purified again. The transfection of modified mRNAs was performed with a TransIT-mRNA transfection kit (Mirus Bio, Madison, WI, USA) following the manufacturer's instruction. Details of the transfection are presented in Table S2. The sizes of all modules involved in this study are listed in Table S3.

Flow cytometry analysis

48 h after transfection, cells were prepared by trypsinizing with 0.05% trypsin at room temperature for 1 min, and then neutralized with Hanks' balanced salt solution (HBSS) containing 2.5 mg/mL bovine serum albumin (BSA). Cells were resuspended and collected for flow cytometry analysis (CytoFLEX, Beckman Coulter, Brea, CA, USA or LSRFortessa, BD Biosciences, Franklin Lakes, NJ, USA). For apoptotic assay, cells were prepared 24 h after transfection. Experiments were repeated three times.

Fluorescent signal quantification from flow cytometric measurements

To maximize the observable reporter range, signal fluorescence was quantified according to Gao et al.[35] dEGFP was chosen as the signal

details are presented in Materials and methods. Blue and red dashed curves indicate the individual Gaussian distributions of the two-component fit, while the purple curve indicates their sum. Area a_0 represents the blue shaded area (the area beneath the blue dashed curve), while area b_0 represents the red shaded area, which means the total area minus area a_0. (F) Calculated reduction index of each group. The index is highly increased in the absence of both HCVp and TEVp. Star represents the reduction index in the absence of both HCVp and TEVp in the first test.

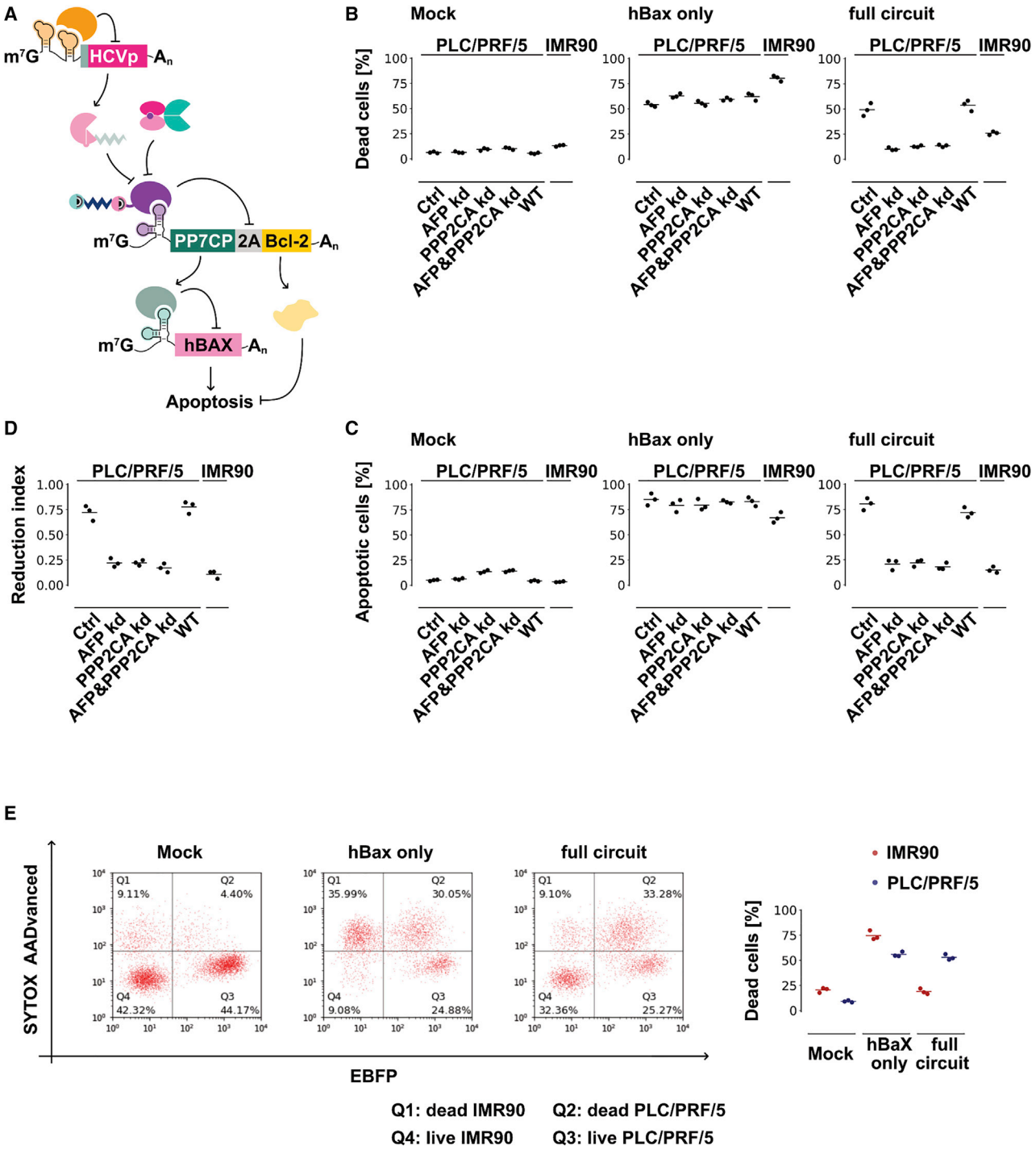

Figure 6. Apoptosis regulatory synthetic circuit specifically kills HCC cells

(A) Schematic representation of the apoptosis regulatory circuit specifically targeting HCC cells. nTEVp-YAP, 14-3-3-cTEVp, and AFP-riboswitch-CZ-HCVp are introduced into the circuit to sense the state of the Hippo pathway and the existence of AFP. (B) Percentage of dead cells in each group. (C) Percentage of apoptotic cells in each group. (D) The synthetic circuit preferentially reduced cell numbers in the PLC/PRF/5 control strain. The knockdown of AFP and PPP2CA, either in combination or alone, decreased the reduction index. (E) Representative flow cytometry assay for cell death in mixed cell culture (IMR90 and PLC/PRF/5) and the percentage of dead cells in each group. PLC/PRF/5 stably expressing EBFP was used to distinguish from IMR90. 24 h after transfection, cells were stained with SYTOX AADvanced and subjected to flow cytometry.

fluorescence while mCherry was chosen as a co-transfection marker. The mCherry signal was used to select highly transfected cells, in which the largest separation was observed between basal reporter fluorescence and cellular autofluorescence. Experiments were repeated three times. The flow cytometry data were processed by Python.

Reduction index calculation from flow cytometric measurements

The reduction index was calculated by comparing the population size of the experimental group to the population size of control group, which was transfected with the fluorescent marker and control circuit. The size of untransfected cells was used as the internal normalization. Experiments were repeated three times. The calculation proceeded according to Gao et al.,[35] except that the flow cytometry data were processed by Python.

Code availability

The flow cytometry data were processed by python (version 3.7.6), the code of which can be accessed in Supplemental materials and methods.

Chemical and photogenetic inducers

ABA (Sigma-Aldrich, St. Louis, MO, USA) was dissolved by DMSO (Solarbio, Beijing, China) at a stock concentration of 50 mM and final concentration at 100 μM. Rapa (Sigma-Aldrich) was dissolved by DMSO at a stock concentration of 1 mM and final concentration at 3 μM. TMP (Sigma-Aldrich) was delivered at 1 μM. ASV (Sigma-Aldrich) was delivered at 3 μM. Parameters for blue light pulses were: 1-s pulse per 3 min, 450 nm, 5.8 mV/cm^2.

siRNAs for gene knockdown

siRNAs used to knockdown AFP (sc-88864), YAP1 (sc-38637), LATS1 (sc-35797), and MOB1B (sc270319) were purchased from Santa Cruz Biotechnology (Dallas, TX, USA). These siRNAs were transfected into 293T or PLC/PRF/5 cells along with modRNAs.

Apoptosis and cell death assay

24 h after transfection, cells were collected and washed with PBS. Cells were then stained with SYTOX red (Life Technologies, Carlsbad, CA, USA) and annexin V-conjugated Alexa Fluor 488 (Life Technologies) at room temperature for 15 min. Experiments were repeated three times. Flow cytometry analysis (LSRFortessa) was used to analyze and detect the state of cells.

Co-culture and cell death assay

PLC/PRF/5 stably expressing EBFP and IMR90 cells were co-cultured. 24 h after transfection, both cells were stained with SYTOX AADvanced (Life Technologies) and then subjected to flow cytometry. Experiments were repeated three times.

Statistical analysis

SciPy library 1.6.1 was used for statistical calculation. Welch's t test was used to evaluate significant differences: $^*p < 0.05$, $^{**}p < 0.01$, $^{***}p < 0.001$; ns, not significant.

SUPPLEMENTAL INFORMATION

Supplemental information can be found online at https://doi.org/10.1016/j.omtn.2021.08.012.

ACKNOWLEDGMENTS

This work was supported by the National Key R&D Program of China (2016YFA0201404) and the National Natural Science Foundation of China (82003254).

AUTHOR CONTRIBUTIONS

J.Y. and S.D. conducted the experiments; J.Y. and S.D. designed the experiments and wrote the paper.

DECLARATION OF INTERESTS

The authors declare no competing interests.

REFERENCES

1. Wu, M.R., Jusiak, B., and Lu, T.K. (2019). Engineering advanced cancer therapies with synthetic biology. Nat. Rev. Cancer *19*, 187–195.
2. Denison, C., and Kodadek, T. (1998). Small-molecule-based strategies for controlling gene expression. Chem. Biol. *5*, R129–R145.
3. Yamada, M., Nagasaki, S.C., Ozawa, T., and Imayoshi, I. (2020). Light-mediated control of gene expression in mammalian cells. Neurosci. Res. *152*, 66–77.
4. Karikó, K., Buckstein, M., Ni, H., and Weissman, D. (2005). Suppression of RNA recognition by Toll-like receptors: The impact of nucleoside modification and the evolutionary origin of RNA. Immunity *23*, 165–175.
5. Sahin, U., Karikó, K., and Türeci, Ö. (2014). mRNA-based therapeutics—Developing a new class of drugs. Nat. Rev. Drug Discov. *13*, 759–780.
6. Tavernier, G., Andries, O., Demeester, J., Sanders, N.N., De Smedt, S.C., and Rejman, J. (2011). mRNA as gene therapeutic: How to control protein expression. J. Control. Release *150*, 238–247.
7. Schott, J.W., Morgan, M., Galla, M., and Schambach, A. (2016). Viral and synthetic RNA vector technologies and applications. Mol. Ther. *24*, 1513–1527.
8. Beckert, B., and Masquida, B. (2011). Synthesis of RNA by in vitro transcription. Methods Mol. Biol. *703*, 29–41.
9. Maruggi, G., Zhang, C., Li, J., Ulmer, J.B., and Yu, D. (2019). mRNA as a transformative technology for vaccine development to control infectious diseases. Mol. Ther. *27*, 757–772.
10. Cella, F., Wroblewska, L., Weiss, R., and Siciliano, V. (2018). Engineering protein-protein devices for multilayered regulation of mRNA translation using orthogonal proteases in mammalian cells. Nat. Commun. *9*, 4392.
11. Liu, K., Yang, J., Ding, S., and Gao, Y. (2020). Daisy chain topology based mammalian synthetic circuits for RNA-only delivery. ACS Synth. Biol. *9*, 269–282.
12. Wroblewska, L., Kitada, T., Endo, K., Siciliano, V., Stillo, B., Saito, H., and Weiss, R. (2015). Mammalian synthetic circuits with RNA binding proteins for RNA-only delivery. Nat. Biotechnol. *33*, 839–841.
13. Van Etten, J., Schagat, T.L., Hrit, J., Weidmann, C.A., Brumbaugh, J., Coon, J.J., and Goldstrohm, A.C. (2012). Human Pumilio proteins recruit multiple deadenylases to efficiently repress messenger RNAs. J. Biol. Chem. *287*, 36370–36383.
14. Ono, H., Kawasaki, S., and Saito, H. (2020). Orthogonal protein-responsive mRNA switches for mammalian synthetic biology. ACS Synth. Biol. *9*, 169–174.
15. Matsuura, S., Ono, H., Kawasaki, S., Kuang, Y., Fujita, Y., and Saito, H. (2018). Synthetic RNA-based logic computation in mammalian cells. Nat. Commun. *9*, 4847.
16. Yamagishi, M., Ishihama, Y., Shirasaki, Y., Kurama, H., and Funatsu, T. (2009). Single-molecule imaging of β-actin mRNAs in the cytoplasm of a living cell. Exp. Cell Res. *315*, 1142–1147.
17. Zalatan, J.G., Lee, M.E., Almeida, R., Gilbert, L.A., Whitehead, E.H., La Russa, M., Tsai, J.C., Weissman, J.S., Dueber, J.E., Qi, L.S., and Lim, W.A. (2015). Engineering

complex synthetic transcriptional programs with CRISPR RNA scaffolds. Cell *160*, 339–350.

18. Wehr, M.C., Laage, R., Bolz, U., Fischer, T.M., Grünewald, S., Scheek, S., Bach, A., Nave, K.A., and Rossner, M.J. (2006). Monitoring regulated protein-protein interactions using split TEV. Nat. Methods *3*, 985–993.
19. Wehr, M.C., Reinecke, L., Botvinnik, A., and Rossner, M.J. (2008). Analysis of transient phosphorylation-dependent protein-protein interactions in living mammalian cells using split-TEV. BMC Biotechnol. *8*, 55.
20. Wehr, M.C., and Rossner, M.J. (2016). Split protein biosensor assays in molecular pharmacological studies. Drug Discov. Today *21*, 415–429.
21. Iwamoto, M., Björklund, T., Lundberg, C., Kirik, D., and Wandless, T.J. (2010). A general chemical method to regulate protein stability in the mammalian central nervous system. Chem. Biol. *17*, 981–988.
22. Taxis, C., Stier, G., Spadaccini, R., and Knop, M. (2009). Efficient protein depletion by genetically controlled deprotection of a dormant N-degron. Mol. Syst. Biol. *5*, 267.
23. Varshavsky, A. (1996). The N-end rule: Functions, mysteries, uses. Proc. Natl. Acad. Sci. USA *93*, 12142–12149.
24. Bartenschlager, R. (1999). The NS3/4A proteinase of the hepatitis C virus: Unravelling structure and function of an unusual enzyme and a prime target for antiviral therapy. J. Viral Hepat. *6*, 165–181.
25. Taremi, S.S., Beyer, B., Maher, M., Yao, N., Prosise, W., Weber, P.C., and Malcolm, B.A. (1998). Construction, expression, and characterization of a novel fully activated recombinant single-chain hepatitis C virus protease. Protein Sci. *7*, 2143–2149.
26. Banaszynski, L.A., Chen, L.C., Maynard-Smith, L.A., Ooi, A.G., and Wandless, T.J. (2006). A rapid, reversible, and tunable method to regulate protein function in living cells using synthetic small molecules. Cell *126*, 995–1004.
27. Ghosh, I., Hamilton, A.D., and Regan, L. (2000). Antiparallel leucine zipper-directed protein reassembly: Application to the green fluorescent protein. J. Am. Chem. Soc. *122*, 5658–5659.
28. Saito, H., Kobayashi, T., Hara, T., Fujita, Y., Hayashi, K., Furushima, R., and Inoue, T. (2010). Synthetic translational regulation by an L7Ae-kink-turn RNP switch. Nat. Chem. Biol. *6*, 71–78.
29. Nallamsetty, S., Kapust, R.B., Tözsér, J., Cherry, S., Tropea, J.E., Copeland, T.D., and Waugh, D.S. (2004). Efficient site-specific processing of fusion proteins by tobacco vein mottling virus protease in vivo and in vitro. Protein Expr. Purif. *38*, 108–115.
30. Endy, D. (2005). Foundations for engineering biology. Nature *438*, 449–453.
31. Han, X., Yang, J., Zeng, F., Weng, J., Zhang, Y., Peng, Q., Shen, L., Ding, S., Liu, K., and Gao, Y. (2020). Programmable synthetic protein circuits for the identification and suppression of hepatocellular carcinoma. Mol. Ther. Oncolytics *17*, 70–82.
32. Meng, Z., Moroishi, T., and Guan, K.L. (2016). Mechanisms of Hippo pathway regulation. Genes Dev. *30*, 1–17.
33. McPhee, F., Friborg, J., Levine, S., Chen, C., Falk, P., Yu, F., Hernandez, D., Lee, M.S., Chaniewski, S., Sheaffer, A.K., and Pasquinelli, C. (2012). Resistance analysis of the hepatitis C virus NS3 protease inhibitor asunaprevir. Antimicrob. Agents Chemother. *56*, 3670–3681.
34. Katz, N., Cohen, R., Solomon, O., Kaufmann, B., Atar, O., Yakhini, Z., Goldberg, S., and Amit, R. (2019). Synthetic 5′ UTRs can either up- or downregulate expression upon RNA-binding protein binding. Cell Syst. *9*, 93–106.e8.
35. Gao, X.J., Chong, L.S., Kim, M.S., and Elowitz, M.B. (2018). Programmable protein circuits in living cells. Science *361*, 1252–1258.
36. Tschaharganeh, D.F., Chen, X., Latzko, P., Malz, M., Gaida, M.M., Felix, K., Ladu, S., Singer, S., Pinna, F., Gretz, N., et al. (2013). Yes-associated protein up-regulates Jagged-1 and activates the Notch pathway in human hepatocellular carcinoma. Gastroenterology *144*, 1530–1542.e12.
37. Wang, S., Zhu, M., Wang, Q., Hou, Y., Li, L., Weng, H., Zhao, Y., Chen, D., Ding, H., Guo, J., and Li, M. (2018). Alpha-fetoprotein inhibits autophagy to promote malignant behaviour in hepatocellular carcinoma cells by activating PI3K/AKT/mTOR signalling. Cell Death Dis. *9*, 1027.
38. Nichols, W.W., Murphy, D.G., Cristofalo, V.J., Toji, L.H., Greene, A.E., and Dwight, S.A. (1977). Characterization of a new human diploid cell strain, IMR-90. Science *196*, 60–63.
39. Khalil, A.S., and Collins, J.J. (2010). Synthetic biology: Applications come of age. Nat. Rev. Genet. *11*, 367–379.
40. Bonnet, J., Yin, P., Ortiz, M.E., Subsoontorn, P., and Endy, D. (2013). Amplifying genetic logic gates. Science *340*, 599–603.
41. Khalil, A.S., Lu, T.K., Bashor, C.J., Ramirez, C.L., Pyenson, N.C., Joung, J.K., and Collins, J.J. (2012). A synthetic biology framework for programming eukaryotic transcription functions. Cell *150*, 647–658.
42. Weinberg, B.H., Pham, N.T.H., Caraballo, L.D., Lozanoski, T., Engel, A., Bhatia, S., and Wong, W.W. (2017). Large-scale design of robust genetic circuits with multiple inputs and outputs for mammalian cells. Nat. Biotechnol. *35*, 453–462.
43. Seo, J.K., Choi, H.S., and Kim, K.H. (2016). Engineering of soybean mosaic virus as a versatile tool for studying protein-protein interactions in soybean. Sci. Rep. *6*, 22436.
44. Weinheimer, S.P., McCann, P.J., 3rd, O'Boyle, D.R., 2nd, Stevens, J.T., Boyd, B.A., Drier, D.A., Yamanaka, G.A., DiIanni, C.L., Deckman, I.C., and Cordingley, M.G. (1993). Autoproteolysis of herpes simplex virus type 1 protease releases an active catalytic domain found in intermediate capsid particles. J. Virol. *67*, 5813–5822.
45. Zheng, N., Pérez, Jde.J., Zhang, Z., Domínguez, E., Garcia, J.A., and Xie, Q. (2008). Specific and efficient cleavage of fusion proteins by recombinant plum pox virus NIa protease. Protein Expr. Purif. *57*, 153–162.
46. Fernandez-Rodriguez, J., and Voigt, C.A. (2016). Post-translational control of genetic circuits using Potyvirus proteases. Nucleic Acids Res. *44*, 6493–6502.
47. Kawasaki, S., Fujita, Y., Nagaike, T., Tomita, K., and Saito, H. (2017). Synthetic mRNA devices that detect endogenous proteins and distinguish mammalian cells. Nucleic Acids Res. *45*, e117.
48. Ausländer, S., Stücheli, P., Rehm, C., Ausländer, D., Hartig, J.S., and Fussenegger, M. (2014). A general design strategy for protein-responsive riboswitches in mammalian cells. Nat. Methods *11*, 1154–1160.
49. Kashida, S., Inoue, T., and Saito, H. (2012). Three-dimensionally designed protein-responsive RNA devices for cell signaling regulation. Nucleic Acids Res. *40*, 9369–9378.